Impact of horizontal resolution on climate model forecasts of tropical precipitation and diabatic heating for the TWP-ICE period

James Boyle

Lawrence Livermore National Laboratory, Livermore, California

Stephen A. Klein

Lawrence Livermore National Laboratory, Livermore, California

J. Boyle, L-103, LLNL/PCMDI, 7000 East Ave, Livermore, CA 94550-9234, (boyle5@llnl.gov)

Abstract. In order to study the impact of horizontal resolution on climate model simulations of tropical moist processes, short term forecasts using the Community Atmospheric Model (version 3.5) at several resolutions are performed for a time period encompassing the Tropical Warm Pool - International Cloud Experiment (TWP-ICE). TWP-ICE occurred in the environment of Darwin, Australia in January and February 2006. The experimental period encompasses a number of atmospheric phenomena, such as an MJO passage , mesoscale convective systems, monsoon trough, and active and dry conditions. The CAM is run with four horizontal resolutions: 2°, 1°, 0.5°, and 0.25° latitude-longitude. Simulated profiles of diabatic heating and moistening at the TWP-ICE site show that the model parameterizations respond reasonably well for all resolutions to the sequence of varying conditions imposed by the analyses used to initialize the model. The global model biases in precipitation are largely unchanged over resolutions and in some regions the 0.25° model displays the largest differences with the observations used.

However, there are substantive positive aspects of finer resolution. The diurnally forced circulations over the Maritime continent are more realistically captured by the 0.25° simulation which is able to better resolve the land-sea breeze. The intensity distribution of rainfall events is also improved at higher resolution through an increased frequency of very intense events and an increased frequency of little or no precipitation. Finally, the ratio of stratiform to convective precipitation systematically increases towards observational es-

timates with increases in resolution. Intriguingly, this appears to result from reduced evaporation of stratiform precipitation in the lower troposphere rather than increased condensation in the upper troposphere.

1. Introduction

This paper assesses the impact of increasing the horizontal resolution of a global climate model on the simulation of tropical moist processes. The horizontal resolution of the model is varied over a factor of eight (0.25° to 2°). The method used is to run the climate model, the Community Atmospheric Model (CAM) version 3.5, in forecast mode and evaluate the short term (24 - 48 h) forecasts against observations. The time period chosen for the forecasts was January and February of 2006 which encompasses the Tropical Warm Pool International Cloud Experiment (TWP-ICE) experiment that was conducted in northern Australia during the monsoon season. The motivation behind the design and execution of TWP-ICE was to better understand the factors that control tropical convection. A comprehensive overview of meteorological and observational aspects of TWP-ICE is provided by *May et al.* [2008]. The observations were organized to provide a comprehensive characterization of the processes occurring on the scale of a typical general circulation model (GCM) grid cell. Figure 1 provides the geography of the experiment. The strategy is to use the observations in the TWP-ICE region to document model performance and as a reference point when examining model performance over the wider Tropics.

There is a long and rich history of experiments addressing the effects of changing the horizontal resolution of GCMs, from which we note the following results that pertain to the simulation of tropical moist processes. *Neale and Slingo* [2003] carried out experiments to investigate the effects of horizontal resolution on tropical rainfall with emphasis on the Maritime Continent (MC). Seventeen year integrations were carried out using the United

Kingdom Meteorological Office HadAM3 GCM at horizontal spacing of 2.5° x 3.75°, 1.67° x 2.5°, 1.25° x1.875° and 0.83° x 1.25° with prescribed monthly mean SSTs. Their results indicate that the diurnal cycle over the islands and the complex circulation patterns generated by land-sea contrasts are crucial for the energy and hydrological cycles of the Maritime Continent and for determining the mean climate of the region. They conclude that at least part of the HadAM3's underestimate of the MC rainfall may be attributable to a poor simulation of the diurnal cycle and the generation of land-sea breezes around the complex system of islands of the region. Common model deficiencies persisted through all the resolutions. *Hack et al.* [2006] performed CAM 3 simulations at T85 (≈1.4°) and T42 (≈2.8°). They found a definite improvement in the model performance at the higher resolution. The greatest impact occurred on the larger scale dynamical circulation. Since the resolved circulation was so much more realistic, it was felt that T85 would be a more suitable vehicle for testing parameterizations. Although the pointwise scale motions were more energetic, the energy of some large scale modes such as the MJO did not reflect a proportional increase to more realistic values. *Lau and Ploshay* [2009] ran simulations of the Geophysical Fluid Dynamics Laboratory (GFDL) AM2 through the same spectrum of resolutions, 2°, 1°, 0.5° , and 0.25°, used in this work. Their focus was on the 0.5° results for the summertime Asian monsoon, especially the East Asian sector. The 0.5° resolution was shown to accurately depict the East Asian frontal systems and the synoptic disturbances that propagate along the front. However, the improved simulation of the mesoscale systems did not lead to a concomitant increase in the accuracy of the precipitation associated with the systems. It was noted that the higher resolution models captured the precipitation modulation produced by topographical forcing, such as the Western Ghats but there were also instances where the higher resolution exacerbated errors in precipitation evident on the coarser grid. *Shaffrey et al.* [2009] compared coupled simulations of the HiGEM (0.83° x 1.25°) and HadGem (1.25° x 1.875°) models developed at the UK Met Office. It was found that the increased resolution provided a better simulation in almost all aspects. The ocean and atmosphere-ocean interactions benefitted the most from the finer grid. They do comment on the refractory nature of the tropical precipitation errors, which are ameliorated by only a small amount in the HiGEM run.

Recently, *Gent et al.* [2009] presented results of decadal coupled simulations at 2° and 0.5° resolutions using a version of CAM quite close to the one in this work. As seen in *Shaffrey et al.* [2009], some of the largest impacts are found in the ocean simulation. *Gent et al.* [2009] report that the SST bias in coastal upwelling regions is reduced by 60%. The precipitation patterns in the Asian monsoon and North America are improved by going from 2° to 0.5° resolution. The authors indicate that a fair portion of the improvement is due to better resolved topography, a similar result to *Lau and Ploshay* [2009]. *Zhao et al.* [2009] demonstrate that a 0.5° resolution calculation using the GFDL model with modified physics parameterizations is capable of simulating the mean climatology and interannual variability of tropical cyclones of which the 2° version was not capable.

A common result in these resolution studies is that the gains in going to higher resolution were fairly moderate. This is not surprising since convection remains unresolved in the finest resolution ($\approx 0.25^\circ$) used. However, many other important processes such as large scale condensation, land-sea interaction, topographical forcing will benefit from the resolved detail. In addition, the finer resolution has the capability to provide more representative dynamical forcing for the convective parameterizations. However imperfect, parameterizations can generally benefit from improved forcing.

This paper brings three new elements to the large body of research on the effects of horizontal grid resolution in a global climate model. First, the climate model is used as a forecast model during a specific observational experiment. This permits verification on a the weather regimes for a specific time period and less reliance on statistical properties. The availability of special observations and analysis during the forecast period allows for the evaluation of the fast physical processes at certain locations with a level of detail often not used in GCM studies. Second, the spectrum of grid model resolutions is wide, 2° to 0.25°, and only one other study [*Lau and Ploshay*, 2009] encompasses this breadth. This spread of resolutions encompasses the range of what is practical for global coupled model research for the immediate future. Finally, a set of integrations were performed with all the resolutions having the exact same settings of some of the poorly constrained aspects of the parameterizations. Models are usually 'tuned' with arbitrary parameter settings varied to achieve in some sense (usually top of atmosphere energy balance) an optimal simulation. Here both tuned and untuned versions of the model are used, permitting a comparison whereby the *only* difference is horizontal grid resolution. This is not to say that tuning the model is in any way suspect; rather running identical versions of the model across resolutions provides a useful perspective when comparing the results.

The next section will describe the observations and weather regimes of the TWP-ICE. This is followed by a description of the models used and the forecast initialization techniques. Next will be presentation of the results, followed by a discussion and conclusions.

1.1. Observations

The TWP-ICE experiment combined aspects of previous observational campaigns, specifically the combination of a dense rawinsonde network and ground based radar and lidar. A part of the observational infrastructure was provided by the Department of Energy (DOE) Atmospheric Radiation Measurement (ARM) Program Climate and Research Facility (ACRF) site (*Ackerman and Stokes* [2003]) and another part included the Australian Bureau of Meteorology instrumentation associated with meteorological research and operational forecasting applications. *May et al.* [2008] list in detail all the instrumentation that was available during the experiment. The basic state variables of wind, temperature and moisture were measured by rawindsondes launched every 3 hours at the stations at the vertices of the polygon drawn in Fig. 1 (at Darwin the sonde frequency was 6 hours). A scanning C-band polarmetric radar (C-POL) located 20 km northeast of Darwin with a range of 150 km provided rainfall estimates within the polygon and tracked the evolution of convective systems. The rawindsonde data was combined with the domain averaged radar precipitation, surface energy fluxes, and top-of-the-atmosphere and surface radiative fluxes to produce an analysis of the large scale dynamical forcing using a variational technique which constrains the sounding data to satisfy column-integrated budgets of mass, energy, and moisture,([*Zhang and Lin*, 1997], [*Zhang et al.*, 2001], [*Xie et al.*, 2010a]). This variational analysis (VA) provides estimates of the profiles of apparent heating (Q_1) and drying (Q_2), [*Yanai et al.*, 1973].

Cloud occurrence profiles were derived from the Millimeter Wavelength (35GHz) Cloud Radar (MMCR), micropulse lidar (MPL), and laser ceilometers using the Active Remotely Sensed Clouds Locations (ARSCL) algorithm of *Clothiaux et al.* [2000]. The ARSCL observations were obtained from the ARM Climate Model Best Estimate archive,[*Xie et al.*, 2010b].

For rainfall observations over the entire Tropics, the Tropical Rainfall Measuring Mission 3B42 (TRMM) data are used, [*Huffman et al.*, 2007] . These are gridded data supplied every 3h at a grid resolution of 0.25° from 50°N to 50°S and represent TRMM observations merged with other satellite estimates. To provide a measure of uncertainty and global coverage, the Global Precipitation Climatology Project (GPCP) rainfall observations were also used, [*Adler et al.*, 2003]. These data are daily means on a 2.5° grid and are a blend of satellite estimates and rain gauge observations.

1.2. Weather during TWP-ICE

Figure 2 presents the ARSCL cloud frequency and two C-POL radar precipitation estimates. The radar rainfall estimates are courtesy of Drs. Courtney Schumacher and Timothy Hume. The Hume data are the values used as input to the variational analysis. The Schumacher rainfall is part of the data used for estimating vertical latent heating profiles from the C-POL radar. These time series provide a backdrop to the synoptic conditions prevalent for the TWP-ICE period. Based on *May et al.* [2008], this paper will divide the experiment period (20 January - 24 February) into three, each determined by the prevailing weather regime, (Table 1). The initial sequence of meteorological conditions was strongly influenced by a MJO event which passed through the experiment region. The period began on 19 January with an active (Wet) monsoon characterized by westerly flow at Darwin and significant precipitation. The cloud cover was extensive with almost constant high level cloud and frequent deep convection. From 19 to 25 January a low formed in the Solomon Sea (9°S, 155°E) and moved west triggering a mesoscale convective system (MCS) that passed through Darwin. This is the very large precipitation event around 24 January, seen in Fig. 2. From 26 January to 2 February, the monsoon tough moved inland and deepened substantially. This initiated the Dry period (at least in the region of Darwin). The movement of the cyclonic center inland resulted in torrential rain south of Darwin and very strong surface westerlies at Darwin. During this period, moderate amounts of rain fell from cumulus congestus clouds which are evident in the ARSCL observations. The Break period, 3 to 13 February, was characterized by a dissipation of the monsoon flow over the Australian/Indonesian region and the development of a heat trough dominating north Australia. Afternoon late day storms formed on the trough / sea breeze boundary. This gave rise to localized, but fairly intense convective events along the coast. Also included in Fig. 2 is the 3h TRMM satellite rainfall estimate averaged over the same area as the radar. This is provided since later evaluations of model of rainfall beyond the TWP-ICE region will use the TRMM estimates. The two estimates of rainfall based on the C-POL radar agree precisely on the timing of rain events, and differ only slightly on the magnitude most of the time. Interestingly, TRMM fails to detect much of the precipitation during the Dry period. This indicates a limitation of the retrieval to discern rain from the middle level topped convection (congestus) present in this period. The TRMM also has several events which exceed the radar estimates by a large fraction.

2. Models

The general GCM used in this work is the Community Atmosphere Model which serves as the atmospheric component of the Community Climate System Model (CCSM). Aside from some minor configuration differences the model used here is that described by *Collins et al.* [2006], with the exception of the two changes made to the parameterization of deep convection and new stratiform cloud microphysics, *Morrison and Gettelman* [2008], *Gettelman et al.* [2008], *Morrison et al.* [2005]. The convective parameterization changes are described in *Neale et al.* [2008] and will be briefly outlined below. All simulations use the finite volume dynamical core with the default 26 layers in the vertical.

The deep convection parameterization in CAM is a bulk mass flux approach described in *Zhang and McFarlane* [1995] (ZM). Closure in the ZM scheme is achieved by a rate limitation on the consumption of Convective Available Potential Energy (CAPE). The default implementation of ZM uses a traditional definition of CAPE which is calculated using an air parcel ascending pseudoadiabatically and not mixing with the environment. The technique used in the new closure,*Neale et al.* [2008], allows mixing of the air parcel with environmental air depending on an assumed entrainment rate. This calculation makes the CAPE sensitive to the moisture profile above the boundary layer. The modification of the CAPE has a significant impact on the frequency and strength of convective events generated by the ZM scheme. The CAM sequentially calls two convective schemes. The first is the ZM scheme described above for penetrative convection and the second is the shallow convective parameterization of *Hack* [1994]. The ZM scheme computes the convective mixing of parcels coming from the lowest level. The Hack scheme is initiated when the parcel in the model layer immediately below is moist adiabatically unstable with respect to the current level. The adjustment to a stable state is accomplished over 3 model layers. As detailed in *Richter and Rasch* [2008], the CAM used here implements a mass-flux parameterization of momentum transport by deep convection based on *Gregory et al.* [1997].

It is common practice to modify aspects of the model parameterizations when horizontal resolution is changed. As discussed by *Hack et al.* [2006], this process usually undertakes to obtain top of the model energy balance that is as close to observational estimates as possible across all model resolutions. A limited number of loosely constrained coefficients in the parameterized processes are varied to accomplish the desired result. In the standard CAM configuration a number of parameters are made functions of horizontal resolution(Table 2). To facilitate a clean comparison, additional integrations were carried out with the 1°, 2° and 0.5° models having the identical settings to the 0.25° model including the time step. The 2° and 1° runs were also run with the recommended resolution dependent parameter settings seen in Table 2 and will be identified as '2°-T' and '1°-T', respectively. Since the only difference in the 0.5° model was the time step, it was judged after some tests not to be worth the resources to run a 'tuned' version for this resolution. It should be mentioned that the convective relaxation time used in the ZM scheme can be made a function of model resolution but in these experiments it is fixed at 1 hour across all resolutions.

The question of how best to compare the observational data at the TWP-ICE site with model output on various model grids is not straightforward. The model grids for the 2° and 0.25° models are shown in Fig. 1. The TWP-ICE observations can be categorized roughly into areal means and point measurements. The region encompassed by the polygon in Fig. 1 was intended to be on the order of a GCM grid cell. Its area is comparable to the coarsest model grid, 2°, used here. Even in this case the comparison is not exact since the model grid does not coincide with the polygon and thus some averaging needs to be done. For all the model grids, the comparison to the TWP-ICE areal mean was performed by taking a weighted mean of grid points surrounding Darwin, the weights being proportional to the area of overlap of the model grid box and the polygon.

2.1. Initialization data and methods

The model was initialized from operational analyses of the European Centre for Medium-Range Weather Forecasts (ECMWF) and National Center for Environmental Prediction (NCEP) Global Data Assimilation System (GDAS) which are available every 6 hours on the native grid of the forecast model. The ECMWF data was on a 1° x 1° latitude-longitude grid with 91 levels on the model hybrid sigma coordinate. The GDAS was on a 0.465° x 0.465°, latitude-longitude grid with 64 levels in the model sigma coordinate. Thus variations at the finest scale of the 0.25° model are generated by CAM and are not directly propagating from the analysis used as the initial condition. The analysis data was interpolated in space to the CAM grid being careful to ensure consistency between the different representation of the surface topography between the CAM and the analyses [*Boyle et al.*, 2008]. The sea surface temperatures used were weekly means based on the National Oceanic and Atmospheric Administration (NOAA) Optimum Interpolation analysis, [*Reynolds et al.*, 2002] and were linearly interpolated in time and space to the model discretization.

The model was run as a NWP forecast model every six hours. The initial conditions for each forecast for wind, temperature, surface pressure and moisture fields are from the analyses and all other atmospheric parameters and land variables are taken from the previous forecast without modification. The land component of the all the models was initialized for the first forecast from a climatological January specific for that model. The idea is to mimic the forecast/analysis cycle carried out at weather forecast centers. The extended forecasts were run for at least 3 days starting from 00GMT. Model output from the second day of these forecasts, hours 24 to 48, are the basis for much of the evaluation undertaken in this paper. The day 2 forecasts are chosen as a compromise between being as close to the observed conditions as possible, but with enough simulation time to be comfortable that any initialization shock is small. When model time series are presented, they represent a concatenation of a series of day 2 forecasts, valid for the times indicated. The ECMWF analyses were used for all the simulations shown here as there did not appear to be any significant dependence on the analyses used to initialize the models.

3. Results

3.1. Rainfall

Figure 3 presents CAM day 2 forecasts and the Hume observational estimates of 3h rainfall over the TWP-ICE polygon for January and February 2006. It is seen that the models depict the time sequence of the observations fairly well, with the higher resolution models capturing the variation more realistically. There is a definite, albeit not large difference between the tuned and untuned 2° and 1° forecasts with the tuned versions appearing to be better. The mean values of the observations for the two months are 9.4, 9.1 and 10.4 mm day^{-1}, for the Hume, Schumacher and TRMM data respectively. The means of the models are generally larger with values of 11, 13, 10, 11.4, 12, and 12.8 mm day^{-1} for the 2°-T, 1°-T, 2°, 1°,0.5° and 0.25° models respectively.

The largest observed rainfall occurs around 24 January 00GMT. This event corresponds to a mesoscale convective system (MCS) passing over Darwin. The model curves all show a lag of 24 hours in peak rainfall for this event, although this is less clear for 0.25°. This most likely results from the analysis data as the ECMWF forecast model precipitation also shows this lag. Similar lagged precipitation also resulted from use of GDAS analysis data. As the MCS circulation cannot be localized in space and time on the scales resolved by all the CAM versions, it should not be expected that the models capture the precise times of convective events although we do expect the models to capture the essential aspects of the clouds and weather for the weather regimes identified above. The models' Day 2 forecasts are slow to capture the rapid diminishment of observed rain from 24 January 00GMT to 25 January 00GMT. The models all show correct timing for the abrupt cessation of rain for two days after 4 February; apparently the large scale forcing dictating this transition is well captured by all resolutions. Examining the effect of resolution, the higher resolution models have greater peak values of precipitation. The 0.25° time series is the only model which exhibits some peaks exceeding the observed. Furthermore, the 0.5° and 0.25° models better depict the variation of the rainfall with the on/off characteristic of the observations whereas the coarser resolution models have rainfall that persists at reduced magnitude between the peaks. Remember that the model rainfall is averaged over the observational polygon of Fig. 1, so that differences in rainfall are not due to looking at a progressively smaller area. All models capture the light rain falling in the dry period between 24 January and 3 February. Note in Fig. 2 that the TRMM data miss the rain over this period. Without the ground radar the models could have been deemed as too wet for these times.

The top row of Fig. 4 displays histograms of hourly averaged precipitation for the 0.25° and 2° models and Hume C-POL radar observations over January and February 2006 for the TWP-ICE polygon. Only data from the two extreme resolution models are shown as the intermediate resolution models evince a fairly systematic progression between these two. The histogram for the 2° model has a tendency to cluster near 10 mm day^{-1} and is more symmetric than the observations. The finer resolution model diminishes the middle peak and spreads out to higher and lower values. While the 0.25° model exhibits better agreement with observations in the incidence of intense precipitation, there is an indication that this model has too much activity at the most intense rain rates of the figure. Consistent with *Field and Shutts* [2009] all models tend to underestimate the occurrence of rain in the lightest categories although this too is partially alleviated by increased resolution. The bottom row of Fig. 4 compares histograms of daily mean rainfall from TRMM and the 0.25° and 2° models in the region of the Maritime continent (95°E to 150°E and 15°S to 15°N). All the data sets were coarse-grained to a 2° x 2° common grid for the comparison. It can be seen that the characteristics of the comparison between models and observations seen at the TWP-ICE location carry over to the larger region. The 0.25° model again produces a more realistic distribution by both adding higher rain rates but also enhancing the very low rates. The negative skewness of the TRMM data over the Maritime continent seen in Fig. 4 originates from observations over land, even though the land is only about 18 percent of the total Maritime continent area.

Figure 5 displays the observed and modeled rainfall for a region enclosing the Maritime continent and Northern Australia averaged over the six day TWP-ICE Wet period. Increasing resolution produces more sharply defined and more intense patterns. More importantly, these patterns are generally in agreement with the observations. An example of resolution improvement is the separate maxima for tropical cyclone Darryl at 120°E, 17°S by the 0.5° simulation.*Zhao et al.* [2009] also observed that tropical cyclones were resolved on a 0.5° grid in a GFDL model. The increasing resolutions tend to fill in detail upon the large scale patterns set up by the 2° model, a characteristic seen in the work of *Lau and Ploshay* [2009] for the GFDL GCM. The 0.25° simulation appears to produce events which are perhaps too intense. During the Break period (not shown) the increased resolution improves the land-sea breeze diurnally forced circulations.

Figure 6 shows the differences of the GPCP daily precipitation and models (Day 2 forecasts) with respect to the TRMM observations averaged over January and February 2006. The pattern of the difference remains quite consistent across all the resolutions. A generalization is that the model overestimates the rainfall in the regions of observed heavy precipitation. This tendency is exacerbated by increasing resolution, particularly across the Pacific on either side of the Equator. This is a signature of the 'split ITCZ' error which is endemic to many climate models and is not alleviated by resolution in this model. The lack of improvement with resolution is consistent with the results of *Pope and Stratton* [2002] who observed that increased resolution could accentuate errors apparent at lower resolutions, and *Lau and Ploshay* [2009] who found that the highest resolution models also exhibited larger precipitation errors at the regional scale.

3.1.1. Diabatic Heating - $\mathbf{Q_1}$

Closely related to the rainfall is the vertical profile of diabatic heating. Figure 7 displays vertical profiles of Q_1 [*Yanai et al.*, 1973] estimates from the variational analysis and the models averaged over the three periods for the TWP-ICE region. It is uncertain exactly how close a correspondence one should demand between the models and observations for Q_1. This quantity is not directly observed but inferred from a number of sometimes poorly known forcings. Furthermore, the complex blend of land and water, islands and mainland make for ambiguities in the site's representation in the lower resolution models. Finally, the experimental period is only 24 days divided into a few weather regimes. Nonetheless, the data available do present an opportunity to evaluate the models over a variety of tropical conditions in a region of importance to the global circulation.

For the Wet period (Fig. 7a) the observational estimate indicates a broad peak centered about 400 hPa. The 2.0° model actually has the best fit to the observations. There is no evidence of a convergence to observations as the grid becomes finer. A number of the models, especially 0.25°, have too much heating. Consideration of the individual parameterizations suggests that the Hack three-level convection scheme is responsible for the lower level discrepancies. As the Hack scheme is activated when moist adiabatically unstable conditions occur, an attempt was made to determine why the 0.25° and 1.0T° models exhibit more instability at the lower levels than the other models. Variables such as advective fluxes of moisture and temperature, latent and sensible heat from the surface were examined but there was no consistent, dominant driver. Comparing the 0.25° and 1°-T, illustrates the complex interaction of parameterizations and model resolution. Changing the parameter settings of the 1° model to be those of the 0.25° results in a Q_1 profile less like the 0.25° and quite similar the coarser 2° and 2°-T simulations.

For the Dry period (Fig. 7b) the heating is considerably reduced by a factor of 4 compared to the Wet period. The observed Q_1 peak shifts to lower levels below 700 hPa. This is consistent with the cloud record of Fig. 2, which indicates that the deep convection of the Wet period was replaced by congestus clouds. All models produce a reduction in heating from the Wet period and also shift the maximum heating to the lower troposphere. The model peak at 900 hPa is due to vertical temperature diffusion. Given the rather weak forcing, the correspondence of models and observations is fairly good and uniform across resolutions.

The Break period (Figs. 7c) has a modest heating peak at a vertical level somewhere between the peaks of the previous periods. The convective cells active during the Break period are isolated events along a land breeze front or over Tiwi Island. As seen in Fig.2, the rain during the Break is more intermittent and weaker than that of the Wet period. The models capture some of the shape of the Q_1 curve but fail to generate enough deep convection to drive the heating above the 500 hPa level . However, there are indications that the higher resolution models are more successful in getting the convection to go deeper.

Overall, the relative shifts in the level of maximum heating between the periods are discernable in the models without any obvious trend due to resolution. This suggests that the convective parameterizations of the model are responding reasonably well to the imposed large scale state from the analyses.

3.1.2. Latent Heating

Figure 8 displays the latent heating rates estimated from radar retrievals over the TWP-ICE polygon, (*Schumacher et al.* [2007],*Frederick and Schumacher* [2008]), averaged over the indicated TWP-ICE periods. The Q_1 from the variational analysis is also plotted. The radar heating estimates are broken out into the contributions by convective and stratiform processes. Although Q_1 and latent heating are not expected to be identical since the Q_1 values include contributions to diabatic heating from radiation and sub-grid sale turbulent fluxes, for these time scales the two should be close above the boundary layer. During the Wet period, the contribution attributed to latent heating by the radar estimate peaks at a slightly lower level than Q_1. The latent heating profiles indicate that the total profile shape is a result of the combination of the stratiform dipole structure and the more dominant convective contribution. This way of producing a top heavy heating profile is described by *Lin et al.* [2004], and is deemed important to maintaining features such as the MJO by *Lin et al.* [2006]. The active phase of an MJO passed though Darwin during the Wet period of TWP-ICE. This combination of heating is also described to be typical for MCSs, (*Houze* [2004], *Schumacher and Houze* [2003]). During the Break and Dry periods, Fig. 8b and 8c, the latent heating is virtually all convective. In both the Wet and Break periods the correspondence between the latent heating and Q_1 is good where the latent heating is expected to dominate the diabatic heating. This tends to validate both data sets, since the vertical structure of the analyzed Q_1 depends on the rawindsonde profiles whereas the vertical structure of the radar latent heating depends on the profiles of radar reflectivity. Note that the Schumacher latent heating profiles are smooth due to the assumed shapes for the heating and because the C-POL has somewhat poorer vertical resolution than the variational analysis sonde data.

Figures 9 and 10 contain model and the observational latent heating rates for the indicated TWP-ICE periods. There is a potential conceptual difference in the heating decomposition of Schumacher and that of the model. The model large-scale represents all resolved grid scale processes while the Schumacher data refers specifically to the stratiform structures associated with mesoscale convective systems. Nonetheless, for an appropriate parameterization suite and sufficient resolution, the model and Schumacher's concept may converge in regions with tropical deep convection.

For the Wet period (Fig. 9a) the observational estimate of the total latent heating indicates a broad peak centered about 450 hPa. The models have a peak that is too high and too large above 400 hPa. For all the models, save 2°, the heating is also too large below the peak. The model convective component , Fig. 9b, is larger below 600 hPa, due to the Hack scheme. This convective overestimate below 600 hPa more than compensates for the exaggerated large scale cooling at the same levels. The peak of the convection is at a slightly lower level than the observational estimates. The large scale dipole, Fig. 9c, is exaggerated in the models, especially at the lower levels. It appears that the models have too much evaporation of the large scale precipitation in the lower troposphere and this is one aspect that become closer to observational estimates as resolution increases.

During the Dry and Break periods, large-scale latent heating plays a minor role in the models and observations and thus only the total latent heating is shown (Fig. 10). During the Dry period, the models underestimate the convective heating above 800 hPa and strongly overestimate it below. From consideration of the individual components this lower level maximum is due to the Hack parmeterization. For the Break period convective heating (Fig. 10b) , the 0.25° and 0.5° models do slightly better in capturing the heating than the lower resolution models with the same parameter settings. This may be because finer resolution allows for a better representation of land sea breeze circulations. For both the Dry and Break periods, the models capture the slight shift in the level of the maxima in the heating profiles.

3.1.3. Large Scale and Convective Precipitation Ratio

Table 3 list the ratios of large scale to total surface precipitation for the models and the observations for the Wet period at TWP-ICE and over the 20°N to 20°S band for January and February. Keep in mind that the definitions of large scale for the observations does not exactly coincide with that of the models as previously discussed, although the agreement in the shape of the profiles in Fig. 9c lends credence to this comparison. As the resolution becomes finer, the ratio also increases to the point that the 0.25° model to exceeds the observational estimate for the TWP-ICE wet period and region. More than half of the increase comes in going from the 0.5° to the 0.25° model. One must be cautious about conclusions from the data in Table 3, the data are from a very small sample of time. Figure 11 displays the ratio of large scale to total rainfall averaged over the latitude band from 20°N to 20°S around the globe for the all the models averaged over January and February 2006. It should be noted that even the models with the largest ratios in Fig. 11 have values somewhat less than TRMM estimates. The observational values, Fig. 3 of *Schumacher and Houze* [2003], analogous to Fig. 11 are on the order of 40% with somewhat less longitudinal variation.

It is interesting to note that the increase in the fraction of precipitation that is large scale can be achieved through parameterization instead of resolution changes. For example, *Lin et al.* [2008] tested a number of convective parameterizations and moisture triggers for atmospheric GCMs. Their model experiments generated a spread of values comparable to Fig. 11, although their results had less longitudinal variation than were found here. *Lin et al.* [2008] also indicate that greater contributions to the large-scale condensation can produce better simulations of convectively coupled equatorial waves. It is also of interest to determine how increased resolution leads to greater large scale precipitation fraction. The standard expectation is that the finer resolution grids make it easier to achieve the threshold relative humidity for stratiform cloud formation and thus could be expected to produce more stratiform rain, as seen in the simulations of *Duffy et al.* [2003] using an earlier version of the CAM. However, the intriguing aspect of the present experiments is that the increase in surface stratiform precipitation is achieved through decreased evaporation in the lower troposphere as resolution increases (Fig. 9b). This maybe because it is easier to saturate smaller gridboxes through precipitation evaporation allowing for a greater fraction of subsequent precipitation formed in the upper troposphere to reach the surface.

3.2. Apparent Drying Q_2

Figure 12 displays the apparent drying (Q_2) [*Yanai et al.*, 1973] for the observations and models for the periods of TWP-ICE. During the Wet period, the higher resolution models are effectively removing water in excess of observed below 500 hPa. This appears to result from an over active Hack convection parameterization whose activity increases with increasing resolution. The 2° models are among the better simulations. Aloft, the models do capture an upper level peak, albeit with a peak at too high a level. The agreement in the other two periods is poor, and the finer grid only appears to exacerbate the problems. The increase in drying in the lower troposphere during the wet period by the finer resolutions is seen to be due to an increase in the Hack removal of water coupled with a decrease in wetting by the large scale. The removal by the deep convection appears to be relatively uniform across the resolutions. During the dry period, the models establish mid-tropospheric evaporation ($Q_2 < 0$)similar to the observations. During the break period the relative shape of the Q_2 profile is reasonably good, but it is not as high as it should be. That is, the model peak at 750 hPa should be at 550 hPa and the model minimum at

900 hPa should be at 800 hPa. As a similar result was found with the break period Q_1, (Fig. 7c) , it appears that the break period convection does not go deep enough.

3.3. Diurnal Variation over the Maritime Continent

The rainfall over the Maritime continent plays a key role in the circulation of the Tropics and the globe, [*Neale and Slingo*, 2003]. The resolution experiments of *Neale and Slingo* [2003] indicate that the diurnal cycle over the islands and the complex circulation patterns generated by land−sea contrasts are crucial for the energy and hydrological cycles of the Maritime Continent and for determining mean climate. Using a regional model of 25 km grid resolution, *Qian* [2008] performed 30 year integrations with prescribed monthly mean SSTs to investigate the nature of the precipitation over the Maritime Continent. He found that the precipitation is concentrated on the islands by diurnally forced sea-breeze convergence, and the under representation of the island topography will result in an underestimate of the region's precipitation. *Arakawa and Kitoh* [2005] found that circulations and rainfall over the Maritime Continent were well simulated by JMA climate model run with approximately 20 km horizontal grid spacing.

Figure 13 shows the mean rainfall from TRMM and the models during January and February at 00 GMT with the daily mean subtracted. 00 GMT is 8AM local time at 120°E and is about the time of the peak of the observed rain over the ocean. The figure shows the aspects of an relative extreme in the land-sea contrasts of the diurnal cycle. *Kikuchi and Wang* [2008] states that the TRMM data used here (3B42) is adequate to describe most aspects of the diurnal cycle and they provide an analysis of the diurnal cycle over the Maritime continent which corresponds well with Fig. 13. The amplitude variation of the peak diurnal variations is over a factor of three in going from the 2° to the 0.25° model. The dipoles which form in the observations about the islands of Java, Sumatra and New Guinea have been shown to be due to gravity currents generated by the uneven heating of mountainous land and ocean and not by advection of the island rain to offshore, [*Arakawa and Kitoh*, 2005]. The model does a good job at high resolution of reducing precipitation over land except in central Borneo where there is an anomalous precipitation maximum. While the increased resolution clearly improves the simulation of the diurnal cycle over this region, this does not translate into correcting the model bias in regional mean rainfall. As seen in Fig. 6, the region has an over estimate of rain with respect to TRMM across all the model resolutions which increases slightly with finer resolution. In all cases, the models overestimate the rain, and if anything this gets worse with increasing resolution. Figure 14 shows the diurnal cycle over land and ocean within the region 95°E to 130°E and 15°S to 15°N from TRMM and the untuned models. The models underestimate the amplitude of the diurnal cycle over both land and ocean by nearly a factor of two when compared to TRMM and this is not improved by increased horizontal resolution. The problem appears to be too much rain by the models during the morning over land leading to a peak in precipitation that is three hours too early and insufficient diminishment of the model rain over the ocean during the early evening. *Neale and Slingo* [2003] expressed an optimism that an improved representation of the diurnal cycle resulting from higher horizontal resolution would improve the model bias. This does not appear to be true for the CAM.

Figure 15 shows the surface divergence and winds at 0 GMT for the models and the GDAS analysis (which we show because it has the finest resolution of the analyses available to us). Higher resolution models capture details of the complex flow between the islands. The diurnal alteration of the surface convergence and divergence becomes very well defined as resolution increases in close correlation to the precipitation. The 0.25° surface divergence compares well with the high resolution GCM results of *Arakawa and Kitoh* [2005] and the regional model simulations of *Qian* [2008] as well as that computed from the GDAS analyses. It appears that resolution of at least 0.5° is required to capture the land-sea breeze circulations about the maritime continent using the CAM.

4. Discussion

The question implicit in any study of climate model resolution is that of assessing what is to be gained by using higher resolution and whether this gain is worth the additional resources. The unsatisfactory answer is that it depends on the context for which the model results are to be used. For the Maritime continent region (Fig. 13) , the areal average rainfall is essentially constant across all the resolutions with an overestimate with respect to TRMM of about 30%. If the main concern is simulating the gross heating in this region, which is important for the global circulation, then the gain represented by an order of magnitude increase in computation expense is marginal. However, if the detailed distribution of rainfall is important then the increased resolution is essential. As found by *Gent et al.* [2009], the better resolved topography drives the model to produce more realistic rainfall patterns in the vicinity of topography. As seen in Figs. 5 and 13, the patterns of rainfall will be quite different in the finer resolution models even if the area averaged bias remains. As pointed out by *Gent et al.* [2009], these pattern changes can have a large effect on the modeled river flows and other aspects of the land hydrology.

It is perhaps telling that the best agreement in the diabatic heating is with the 2° models (Fig. 7). This might be due to the fact that most development effort has been carried out at this resolution. Nonetheless, a factor of eight increases in resolution had a relatively minor impact on this important field. Also of note is the fact that the 1°-T behaved so differently from the untuned version. As the 1° untuned model shares the same settings as the 0.25° and 0.5° models, one might expect this model to be more similar to the finer resolution models but the opposite situation is found. This would seem to illustrate that tuning can be an effective means to produce better simulations and can have substantial impacts on model performance. *Pope and Stratton* [2002] indicate that parameterizations probably need to be revised or replaced as resolution increases due to non-linear effects that can generate errors unique to each resolution. Indeed, our results suggest that the Hack convection scheme is unduly sensitive to horizontal resolution and should be revised or removed (as it will be in a future version of CAM). We note that the 0.25° model has had only a small amount of development and thus continued exploration of parameter settings in climate and forecast integrations could lead to substantial improvements.

Despite little change in the area-averaged rainfall, we note the following improvements with higher horizontal resolution. First, CAM produced diurnal circulations that appear to be as least as realistic as leading NWP forecast centers and regional models for the Maritime Continent. Second, CAM also shows an increase in the ratio of stratiform to convective rainfall with increased resolution, which should have a positive impact on convectively coupled waves [*Lin et al.*, 2008]. Finally, the temporal variability and intensity of rainfall is more realistic at higher resolution as seen in the time series of Fig. 3.

5. Conclusions

The CAM 3.5 with Morrison and Gettleman microphysics was run as a forecast model starting from ECMWF and NCEP global analyses. The model was run for the period of January and February 2006 during which the TWP-ICE experiment provided detailed heating profiles and precipitation data for the region ($\approx 1.5°$ radius) about Darwin, Australia. Day 2 forecast results were analyzed and allow the model parameterizations to be evaluated outside of model biases which will develop in longer term climate integrations. The model was run with nominal horizontal resolutions of 2°, 1°, 0.5°, and 0.25° and 26 vertical levels. Analysis of the integrations showed that the CAM is capable of producing credible simulations across a broad range of resolutions. Tuning the model generally improves the simulations, but the model response to tuning is complex and the choice of the final parameter values will probably require substantial effort. Circulation features such as tropical cyclones were somewhat more realistically represented in the 0.5° and 0.25° simulations compared to the coarser models.

Compared to the heating profiles computed for the TWP-ICE experiment, the model produced very credible simulations when consideration is taken for the uncertainty endemic to these observations. Particularly encouraging is the generally good simulation of heating profiles in very different weather regimes, which indicates that the model's parameterizations respond properly to the change in large scale state imposed by the analyses. There was no obvious progression toward the observations in the heating rates across resolutions except in that the depth of land-sea breeze convection during the break period is greater and closer to observed with higher resolution.

The global biases of precipitation with respect to the TRMM observations had very similar patterns across resolutions, and the agreement did not improve with increasing resolution. There was a systematic shift towards observational estimates of the ratio of convective to large scale rainfall as resolution was increased. Additionally, the model simulated reasonable vertical profiles of large scale and convective heating and their relative amounts. The spatial pattern of diurnal variation of rainfall and surface wind over the Maritime continent demonstrated a dramatic improvement at finer resolution. For this aspect of the simulations the 0.25° model compared favorably to published regional integrations and operational NWP forecasts.

Acknowledgments. We are grateful to the European Center for Medium Range Weather Forecasts and National Center for Environmental Prediction for making their operational analyses available. Dr. Courtney Schumacher generously supplied latent heating estimates for the TWP-ICE. Timothy Hume provided high resolution precipitation data for the months of January and February 2006. Thanks to Peter Caldwell and Shaocheng Xie for providing comments on the manuscript. The variational analyses and other observational data were obtained from the ARM program sponsored by the U. S. Department of Energy, Office of Science, Office of Biological and Environmental Research, Environmental Sciences Division. Work at LLNL was performed under the auspices of the U. S. Department of Energy by Lawrence Livermore National Laboratory under contract No. DE-AC52-07NA27344. The efforts of the authors were funded by the Regional and Global Climate Modeling and Atmospheric System Research programs of the U. S. Department of Energy as part of the Cloud-Associated Parameterizations Testbed (CAPT).

References

Ackerman, T. P., and G. Stokes (2003), The Atmospheric Radiation Measurement Program, *Phys. Today*, *56*, 38–45.

Adler, R. F., et al. (2003), The version-2 Global Precipitation Climatology Project (GPCP) monthly precipitation analysis (1979-present), *Journal of Hydrometeorology*, *4*(6), 1147–1167.

Arakawa, O., and A. Kitoh (2005), Rainfall diurnal variation over the indonesian maritime continent simulated by 20 km-mesh GCM, *SOLA*, *1*, 109–112.

Boyle, J., S. Klein, G. Zhang, S. Xie, and X. Wei (2008), Climate model forecast experiments for TOGA COARE, *Mon. Wea. Rev*, *136*, 808–832.

Clothiaux, E. E., T. P. Ackerman, G. G. Mace, K. P. Moran, R. T. Marchand, M. A. Miller, and B. E. Martner (2000), Objective determination of cloud heights and radar reflectivities using a combination of active remote sensors at the ARM CART sites, *Journal of Applied Meteorology*, *39*(5), 645–665.

Collins, W. D., et al. (2006), The formulation and atmospheric simulation of the Community Atmosphere Model version 3 (CAM3), *Journal of Climate*, *19*(11), 2144–2161.

Duffy, P. B., B. Govindasamy, J. P. Iorio, J. Milovich, K. R. Sperber, K. E. Taylor, M. F. Wehner, and S. L. Thompson (2003), High-resolution simulations of global climate, part 1: present climate, *Climate Dynamics*, *21*, 371–390.

Field, P. R., and G. J. Shutts (2009), Properties of normalised rain-rate distributions in the tropical Pacific, *Q. J. R. Meteorol. Soc.*, *135*, 175–186.

Frederick, K., and C. Schumacher (2008), Anvil characteristics as seen by C-POL during the Tropical Warm Pool International Cloud Experiment (TWP-ICE), *Monthly Weather Review*, *136*(1), 206–222.

Gent, P. R., S. G. Yeager, R. B. Neale, S. Levis, and D. A. Bailey (2009), Improvements in a half degree atmosphere/land version of the CCSM, *Climate Dyn.*

Gettelman, A., H. Morrison, and S. J. Ghan (2008), A new two-moment bulk stratiform cloud microphysics scheme in the Community Atmosphere Model, Version 3 (CAM3). part II: Single-column and global results, *Journal of Climate*, *21*(15), 3660–3679.

Gregory, D. R., R. Kershaw, and P. M. Inness (1997), Parametrization of momentum transport by convection II: Tests in single-column and general circulation models, *Quart. J. Roy. Meteor. Soc.*, *123*(1153-1183).

Hack, J., J. M. Caron, G. Danabasoglu, K. W. Oleson, C. Bitz, and J. Truesdale (2006), CCSM-CAM3 climate simulation sensitivity to changes in horizontal resolution, *Journal of Climate*, *19*(11), 2267–2289.

Hack, J. J. (1994), Parmeterization of moist convection in the National Center for Atmospheric Research Community Climate Model (CCM2)., *J. Geophys. Res.*, *99*, 5551–5568.

Houze, J., Robert A. (2004), Mesoscale convective systems, *Rev. Geophys.*, *42*.

Huffman, G. J., R. F. Adler, D. T. Bolvin, G. Gu, E. J. Nelkin, K. P. Bowman, Y. Hong, E. F. Stocker, and D. B. Wolff (2007), The TRMM multisatellite precipitation analysis (tmpa): Quasi-global, multiyear, combined-sensor precipitation estimates at fine scales, *Journal of Hydrometeorology*, *8*(1), 38–55.

Kikuchi, K., and B. Wang (2008), Diurnal precipitation regimes in the global tropics, *Journal of Climate*, *21*(11), 2680–2696.

Lau, N.-C., and J. J. Ploshay (2009), Simulation of synoptic- and subsynoptic-scale phenomena associated with the East Asian summer monsoon using a high-resolution GCM, *Monthly Weather Review*, *137*(1), 137–160.

Lin, J., B. Mapes, M. Zhang, and M. Newman (2004), Stratiform precipitation, vertical heating profiles, and the Madden Julian oscillation, *Journal of the Atmospheric Sciences*, *61*(3), 296–309.

Lin, J.-L., M.-I. Lee, D. Kim, I.-S. Kang, and D. M. W. Frierson (2008), The impacts of convective parameterization and moisture triggering on AGCM-simulated convectively coupled equatorial waves, *Journal of Climate*, *21*(5), 883–909.

Lin, J.-L., et al. (2006), Tropical intraseasonal variability in 14 IPCC AR4 climate models. part I: Convective signals, *Journal of Climate*, *19*(12), 2665–2690.

May, P. T., J. H. Mather, G. Vaughan, C. Jakob, G. M. McFarquhar, K. N. Bower, and G. G. Mace (2008), The tropical warm pool international cloud experiment, *Bulletin of the American Meteorological Society*, *89*(5), 629–645.

Morrison, H., and A. Gettelman (2008), A new two-moment bulk stratiform cloud microphysics scheme in the community atmosphere model, version 3 (cam3). part i: Description and numerical tests, *Journal of Climate*, *21*(15), 3642–3659.

Morrison, H., J. A. Curry, and V. I. Khvorostyanov (2005), A new double-moment microphysics parameterization for application in cloud and climate models. part i: Description, *Journal of the Atmospheric Sciences*, *62*(6), 1665–1677.

Neale, R., and J. Slingo (2003), The maritime continent and its role in the global climate: A GCM study, *Journal of Climate*, *16*(5), 834–848.

Neale, R. B., J. H. Richter, and M. Jochum (2008), The impact of convection on ENSO: From a delayed oscillator to a series of events, *Journal of Climate*, *21*(22), 5904–5924.

Pope, V. D., and R. A. Stratton (2002), The processes governing horizontal resolution sensitivity in a climate model, *Climate Dynamics*, *19*, 211–236.

Qian, J.-H. (2008), Why precipitation is mostly concentrated over islands in the maritime continent, *Journal of the Atmospheric Sciences*, *65*(4), 1428–1441.

Reynolds, R., N. Rayner, T. Smith, D. Stokes, and W. Wang (2002), An improved in situ and satellite SST analysis for climate., *J. Climate*, *15*, 1609–1625.

Richter, J. H., and P. J. Rasch (2008), Effects of convective momentum transport on the atmospheric circulation in the community atmosphere model, version 3, *Journal of Climate*, *21*(7), 1487–1499.

Schumacher, C., and R. A. Houze (2003), Stratiform rain in the tropics as seen by the TRMM precipitation radar, *Journal of Climate*, *16*(11), 1739–1756.

Schumacher, C., M. H. Zhang, and P. E. Ciesielski (2007), Heating structures of the TRMM field campaigns, *Journal of the Atmospheric Sciences*, *64*(7), 2593–2610.

Shaffrey, L. C., et al. (2009), U.K. HiGEM: The new U.K. high-resolution global environment model-model description and basic evaluation, *Journal of Climate*, *22*(8), 1861–1896.

Xie, S., T. Hume, C. Jakob, S. A. Klein, R. B. McCoy, and M. Zhang (2010a), Observed large-scale structures and diabatic heating and drying profiles during twp-ice, *Journal of Climate*, *23*(1), 57–79.

Xie, S., et al. (2010b), CLOUDS AND MORE: ARM climate modeling best estimate data, *Bulletin of the American Meteorological Society*, *91*(1), 13–20.

Yanai, S., M., Esbensen, and J.-H. Chu (1973), Determination of bulk properties of tropical cloud clusters from large-scale heat and moisture budgets, *J. Atmos. Sci.*, *30*, 611–627.

Zhang, G. J., and N. A. McFarlane (1995), Sensitivity of climate simulations to the parameterization of cumulus convection in the Canadian Climate Centre general circulation model, *Atmos. Ocean*, *33*, 407–446.

Zhang, M. H., and J. L. Lin (1997), Constrained variational analysis of sounding data based on column-integrated budgets of mass, heat, moisture, and momentum: Approach and application to ARM measurements, *Journal of the Atmospheric Sciences*, *54*(11), 1503–1524.

Zhang, M. H., J. L. Lin, R. T. Cederwall, J. Yio, and S. C. Xie (2001), Objective analysis of ARM IOP data. methods and sensitivity, *Mon. Wea. Rev.*, *120*(1), 295–311.

Zhao, M., I. M. Held, S.-J. Lin, and G. A. Vecchi (2009), Simulations of global hurricane climatology, interannual variability, and response to global warming using a 50-km resolution gcm, *Journal of Climate*, *22*(24), 6653–6678.

Wet Monsoon (Active)	Dry Monsoon	Break
20 January - 25 January	26 January - 2 February	3 February - 13 February

Table 1. Time periods used for averaging over the TWP-ICE.

variable	1.9° x 2.5°	0.9° x 1.25°	0.47° x 0.63°	0.23° x 0.31°
Threshold for autoconversion of cold ice (unitless)	9.5e6	18.0e6	45.0e6	45.0e6
Rain water autoconversion coefficient -Hack scheme (m^{-1})	1.0e-4	1.0e-4	5.0e-5	5.0e-5
time step (seconds)	1800s	1800s	1800s	900s

Table 2. CAM resolution dependent parameters. The default settings are shown. The 2°-T and 1°-T 'tuned' models used the 1.9° x 2.5° and 0.9° x 1.25° settings, respectively. The other models, 2°, 1°, 0.5°, and 0.25° used the setting show for the 0.23° x 0.31° line.

model	TWP-ICE Wet period	20°N to 20°S for January and February 2006
1.9° x 2.5° Tuned	6	10
1.9° x 2.5°	11	13
0.9° x 1.25° Tuned	14	10
0.9° x 1.25°	15	14
0.47° x 0.63°	18	19
0.23° x 0.31°	39	28
Schumacher Obs	32	≈ 40

Table 3. Ratio of the large scale (stratiform for Obs) to total rainfall at TWP-ICE for the Wet period and for the tropical region 20°N to 20°S over January and February 2006. Units are %.

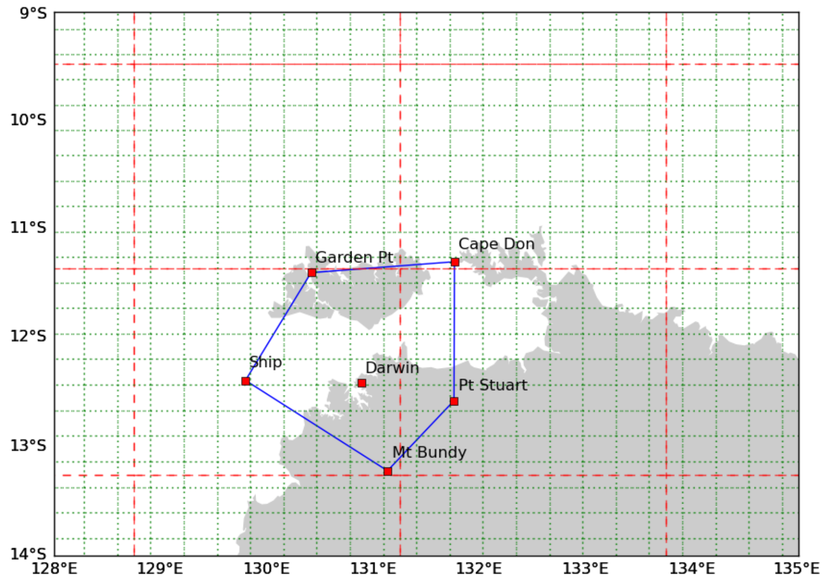

Figure 1. Locator map for key sites of the Tropical Warm Pool – International Cloud Experiment(TWP-ICE). The rawindsonde and surface data were collected at the stations on the vertices of the polygon. Darwin was the site of the precipitation and cloud radar as well as a rawindsonde and surface station. The radar precipitation estimates are for the region encompassed by the polygon. The dotted green lines are the boundaries of the 0.25° model grid and the dashed red lines are the boundaries of the 2° model grid.

.

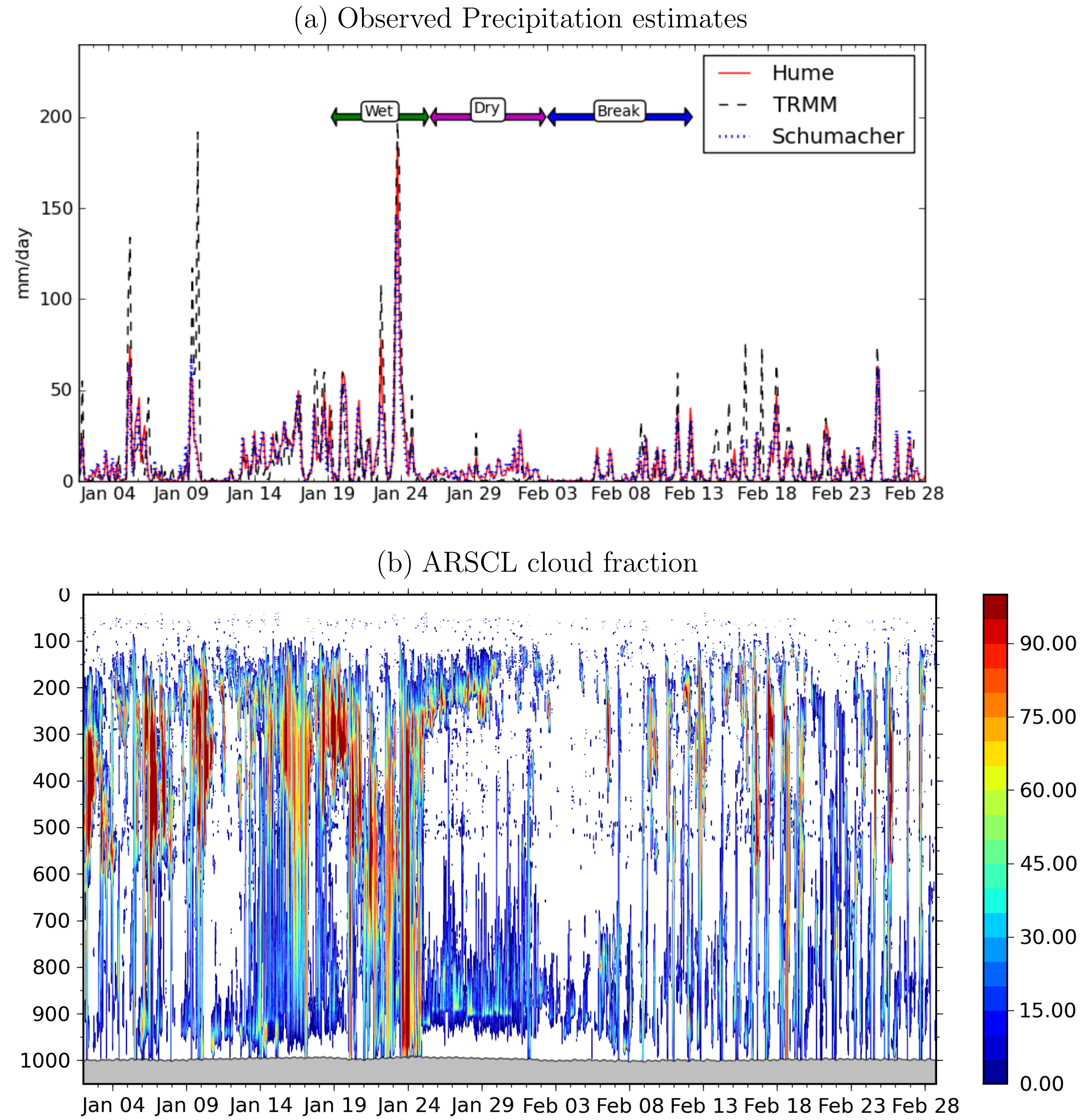

Figure 2. (a) Precipitation estimates from the C-POL radar (Hume and Schumacher) and TRMM averaged over TWP-ICE polygon, (mm day^{-1}) and Observed Cloud Frequency (ARSCL) at Darwin from the ARM cloud radar (percent) . The C-POL radar observations are for 1 h intervals for the TWP-ICE polygon. TRMM estimates are a combination of satellite and ground based observations and are for 3 h intervals. The extents of the subperiods chosen for the TWP-ICE experiment are indicated on the precipitation plot.

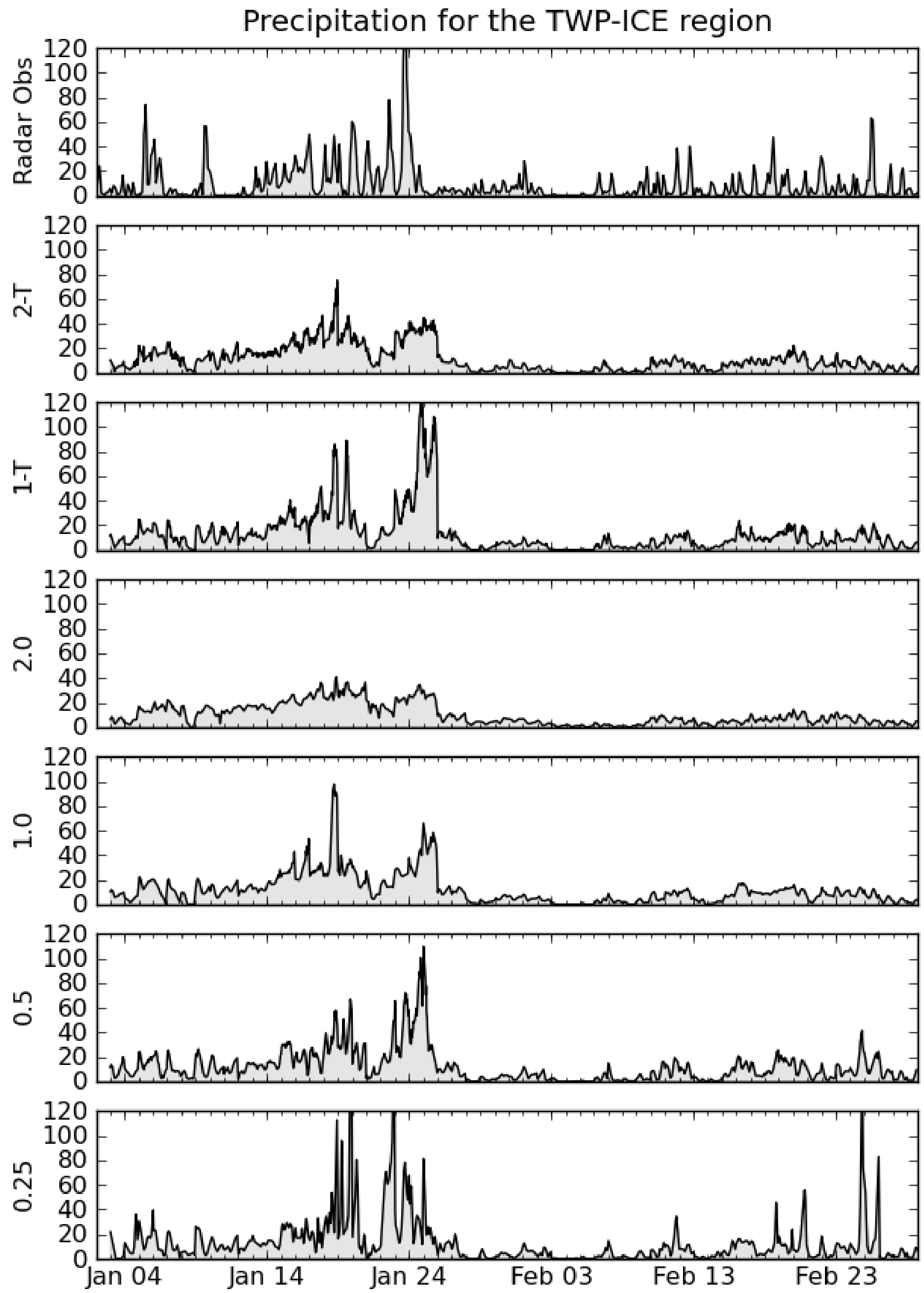

Figure 3. Radar-estimated (Hume) and modeled rainfall for January and February 2006. Data are for one hour means within the TWP-ICE polygon. Units are mm day^{-1}.

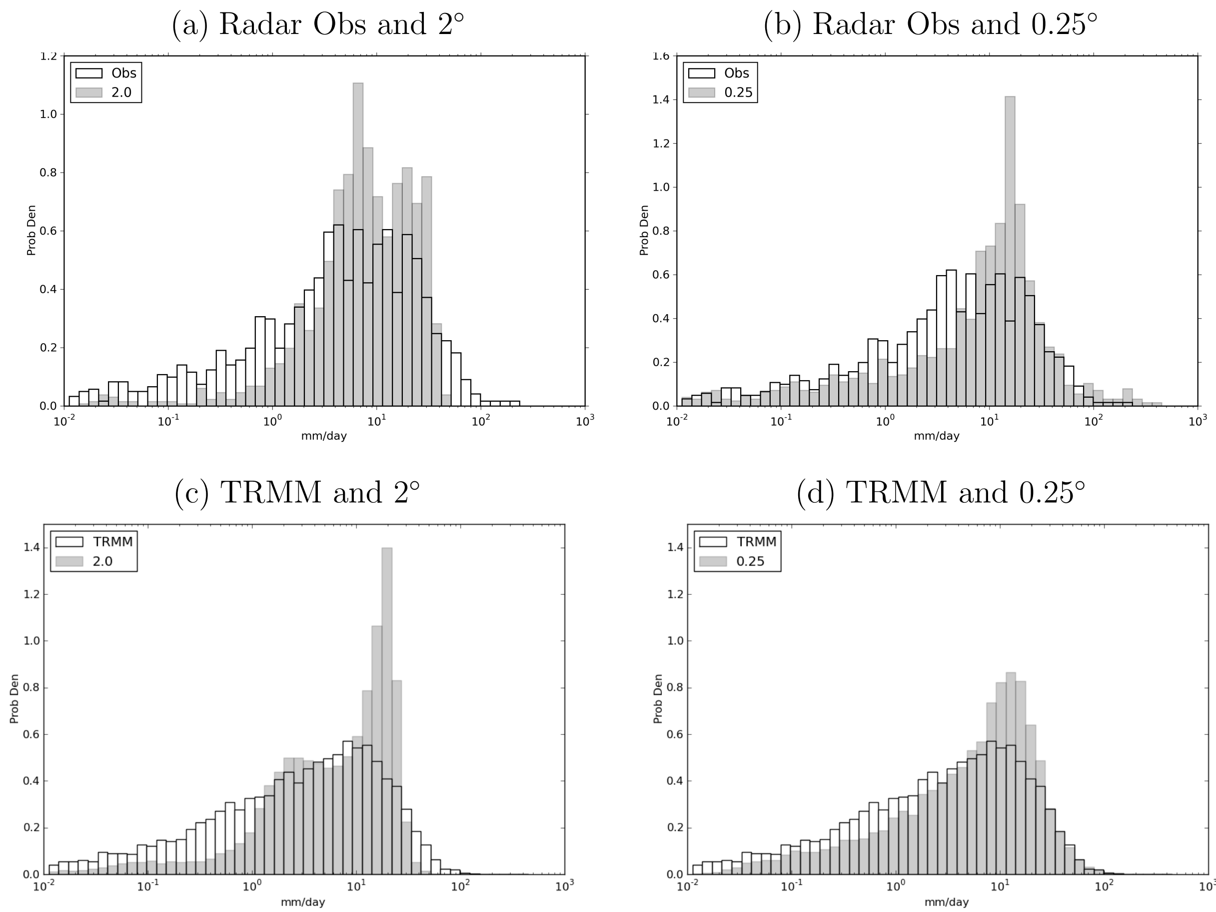

Figure 4. Histograms of observed and modeled rainfall for January and February 2006. Top row(a,b) displays C-POL radar hourly estimates and model data for the TWP-ICE polygon. The lower row (c,d) display daily means for the region 15°S to 15°N,105°E to 155°E (Maritime Continent) from TRMM observations and model data. For the lower row, both the models and TRMM are coarse-grained to a common 2° x 2° grid before computing the histogram. Units are mm day^{-1}.

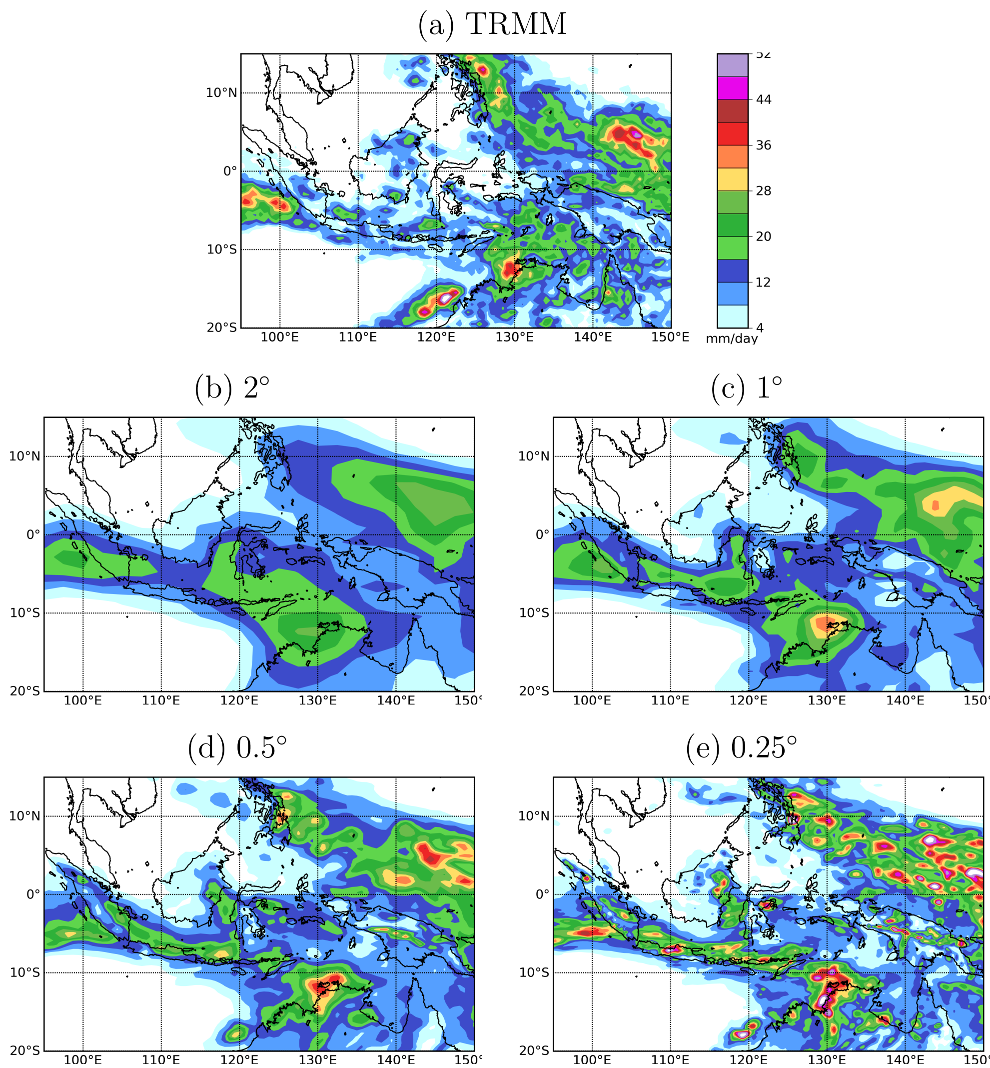

Figure 5. TRMM and modeled rainfall for the Maritime continent region averaged over the six day TWP-ICE Wet period. Units are mm day^{-1}.

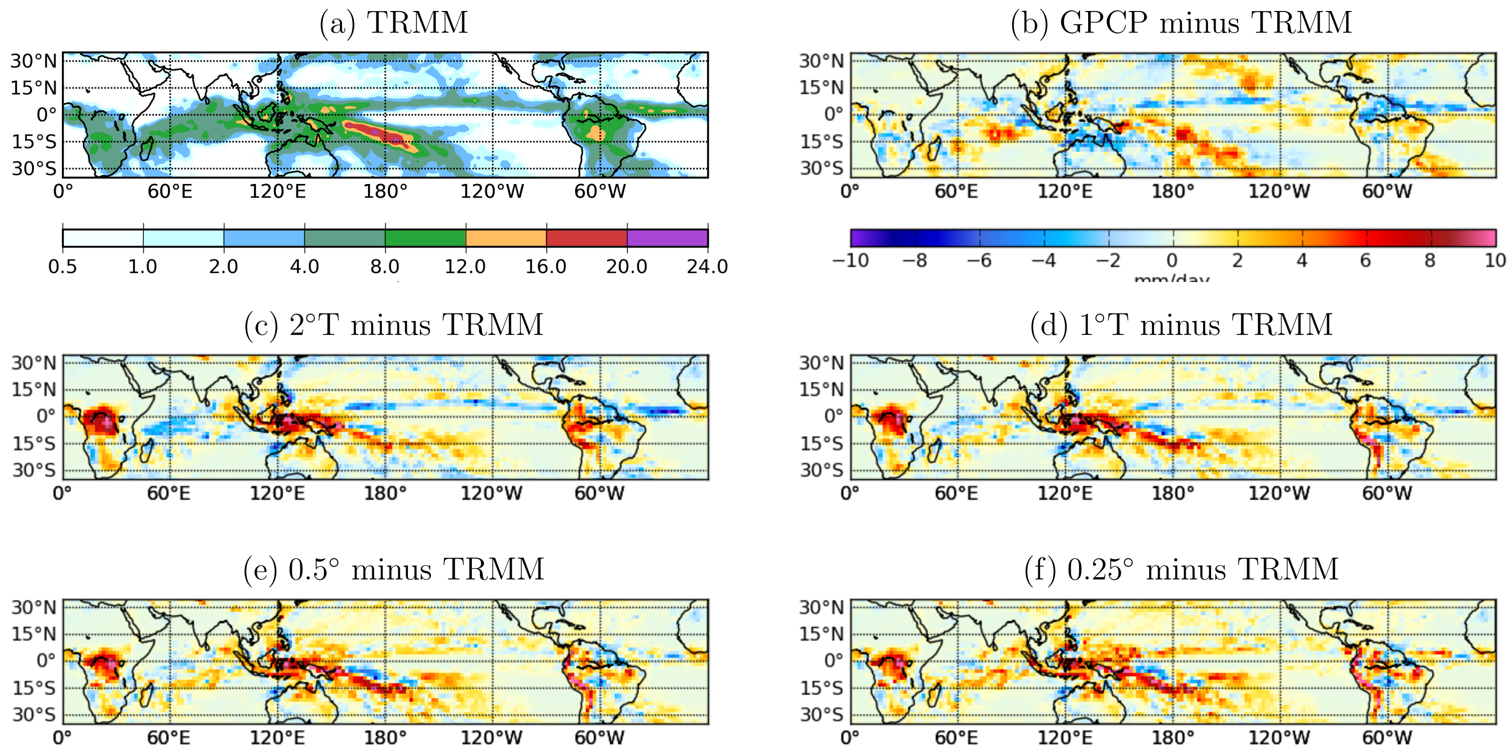

Figure 6. TRMM observed Rainfall (a) and differences GPCP and model differences (b to f) from TRMM for January and February 2006. Units are mm day $^{-1}$. All difference plots (b through f) use the same color scale as in (b)

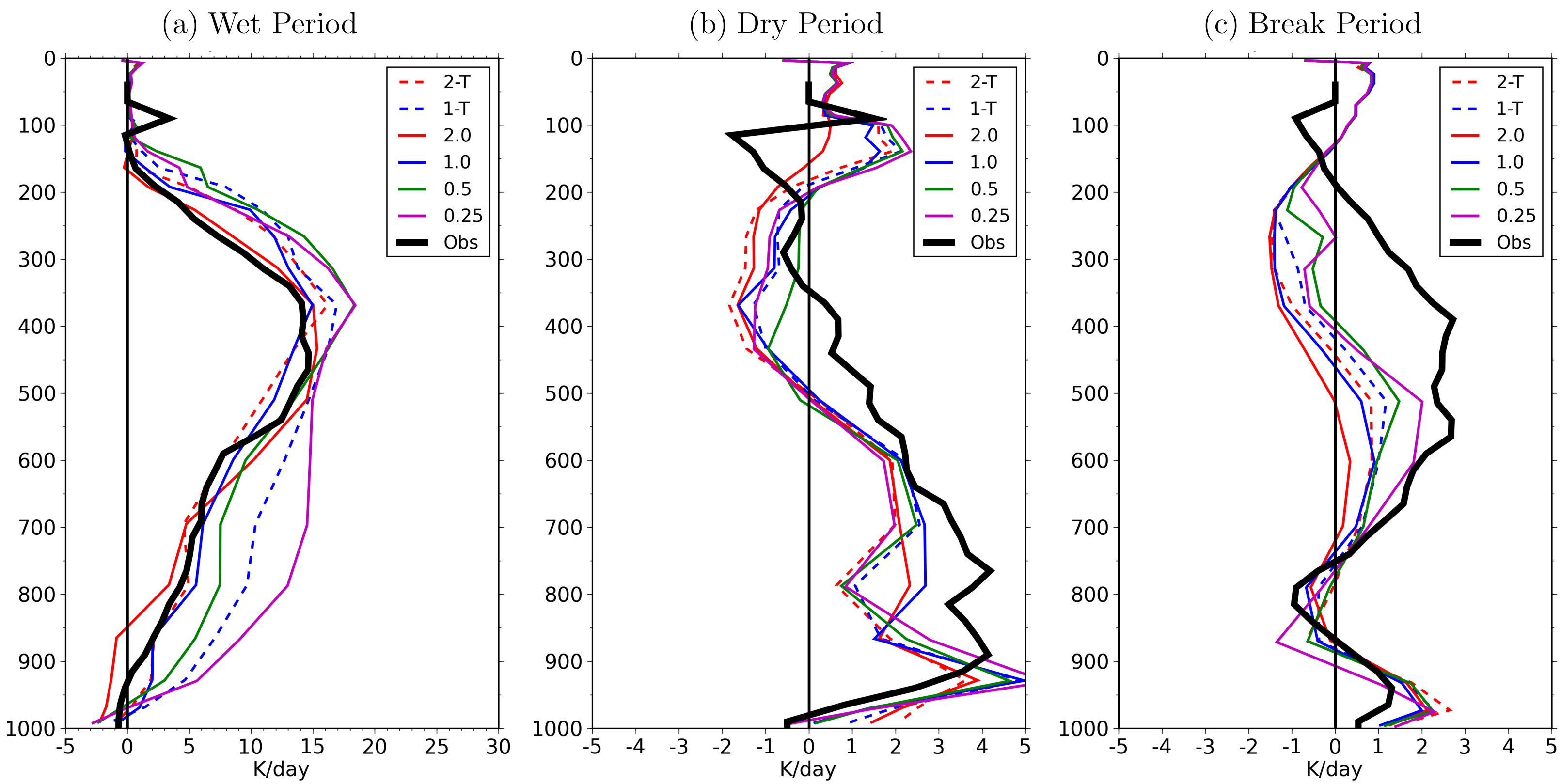

Figure 7. Variational Analysis Obs and modeled apparent heating for the TWP-ICE Wet (a), Dry (b) and Break (c) periods. Note the change in scale between panels (a) and (b−c). Units are °K day^{-1}.

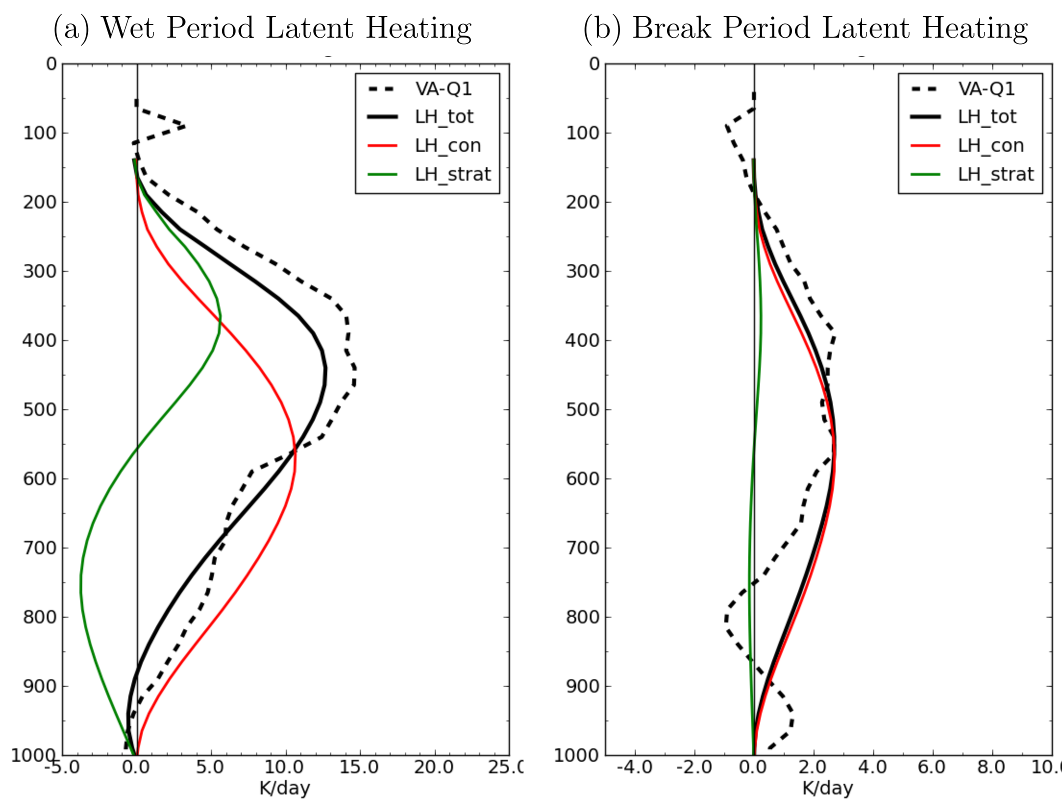

Figure 8. Radar estimated latent heating over the TWP−ICE region for the Wet and Break Periods. Contributions to the heating are divided in stratiform (LH_strat), convective(LH_con) and total (LH_tot). Also shown is the Q_1 from the variational analysis (VA−Q1). Units are °K day^{-1}.

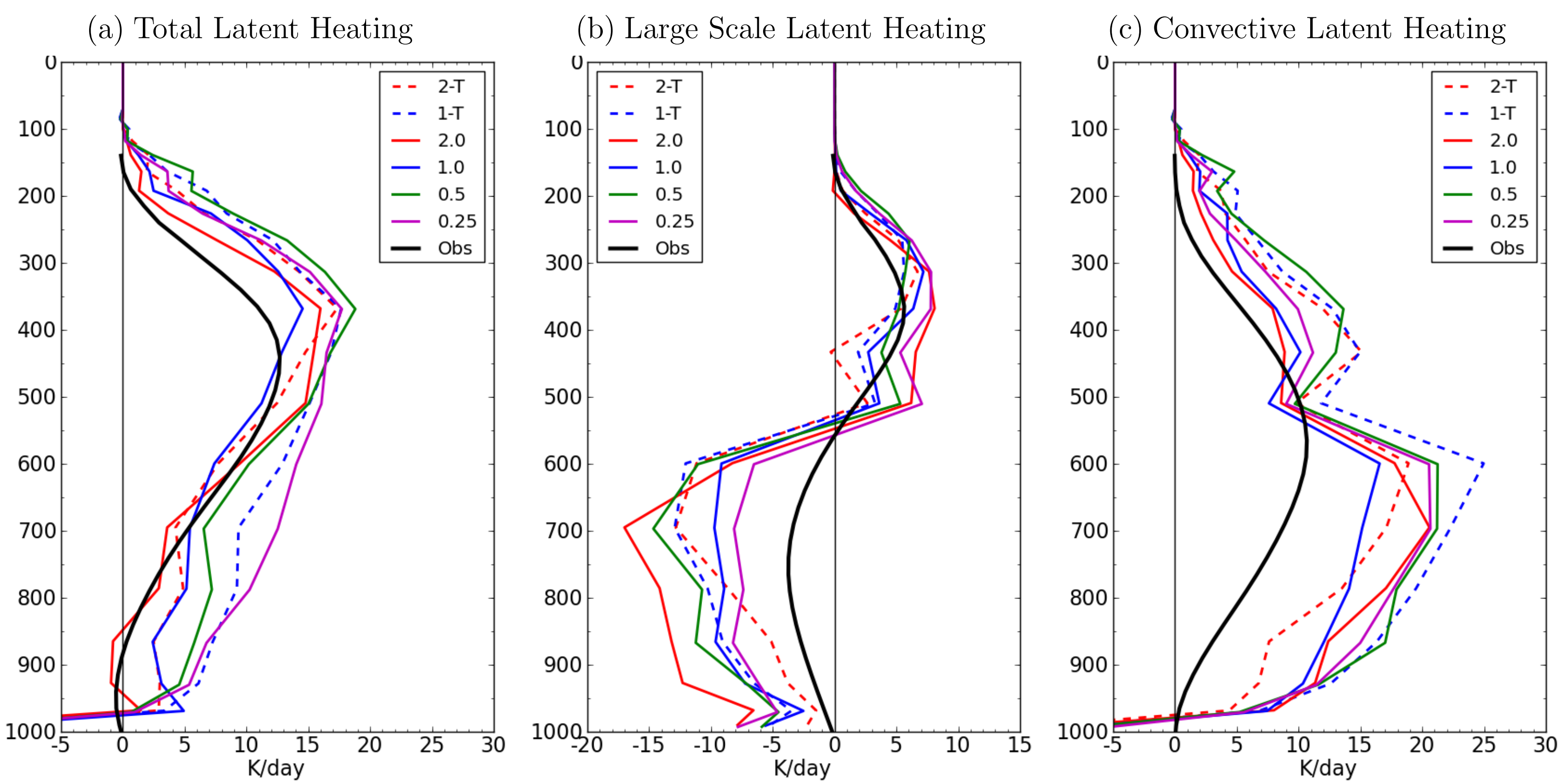

Figure 9. Radar estimated and modeled latent heating over the TWP-ICE polygon for the Wet Period. Contributions to the total heating (a) are divided in large scale (b), and convective (c). Units are $^{\circ}$K day^{-1}.

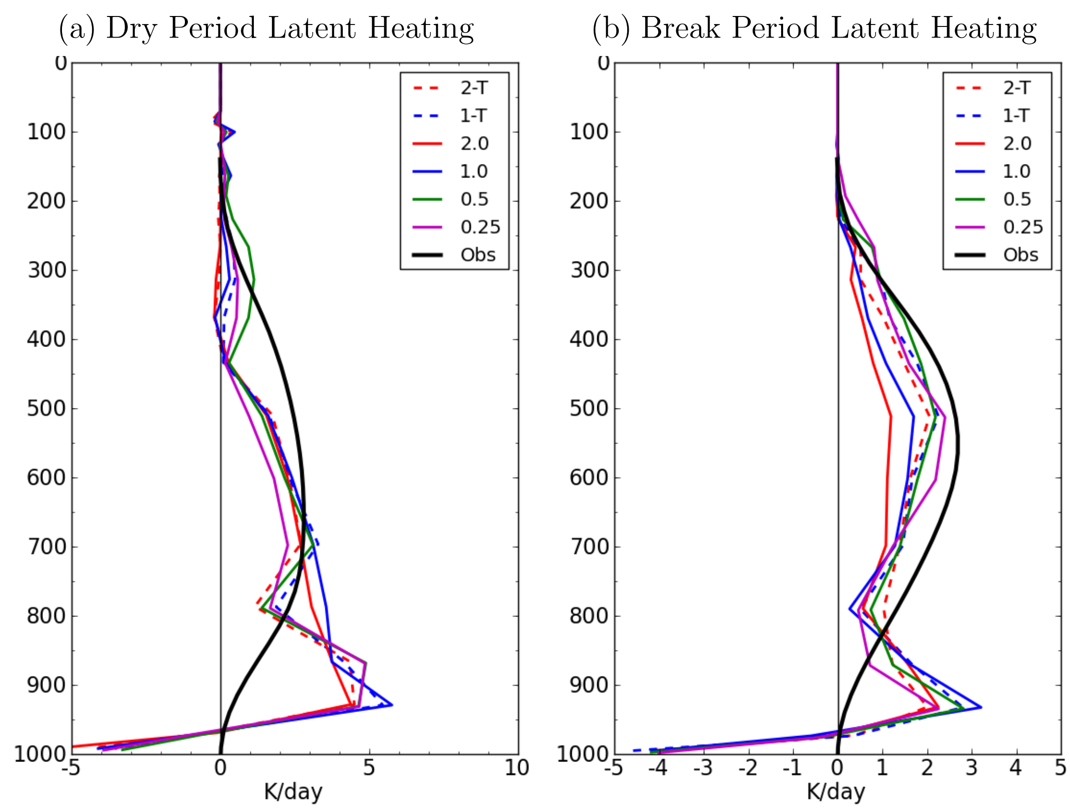

Figure 10. Radar estimated and modeled latent heating over the TWP-ICE polygon for the Dry (a) and Break (b) Period. Only the total heating (convective + large scale) is presented. Units are °K day^{-1}.

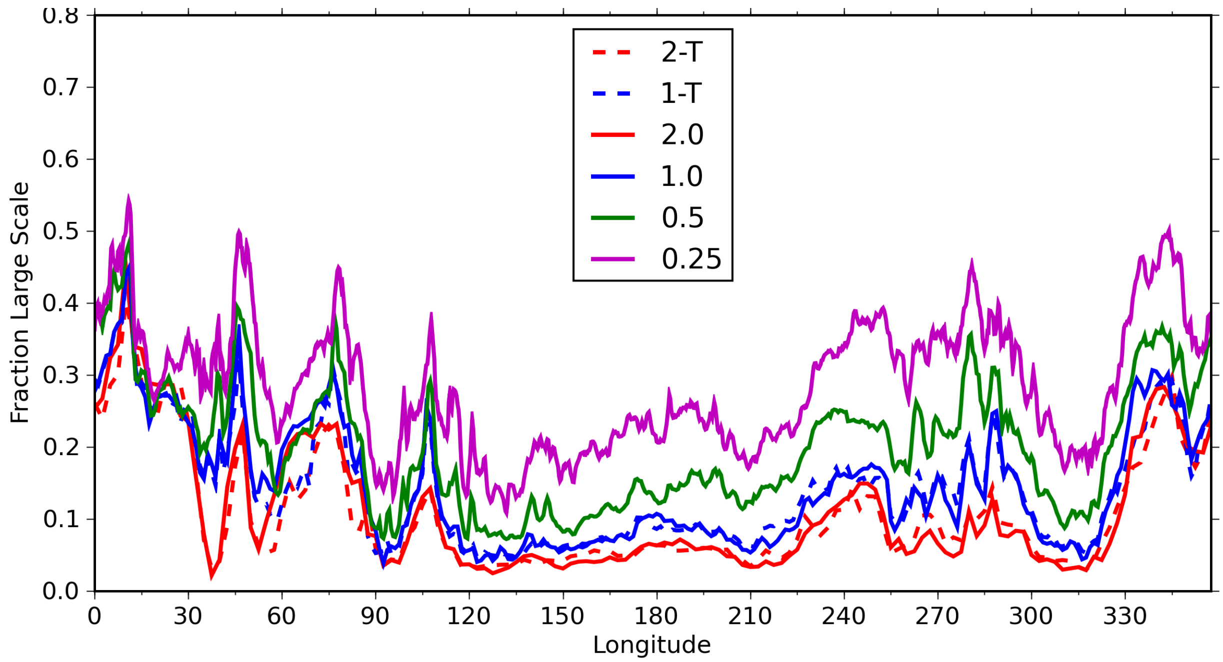

Figure 11. Model fraction of large scale precipitation compared to total precipitation averaged from 20°S to 20°N for January and February 2006.

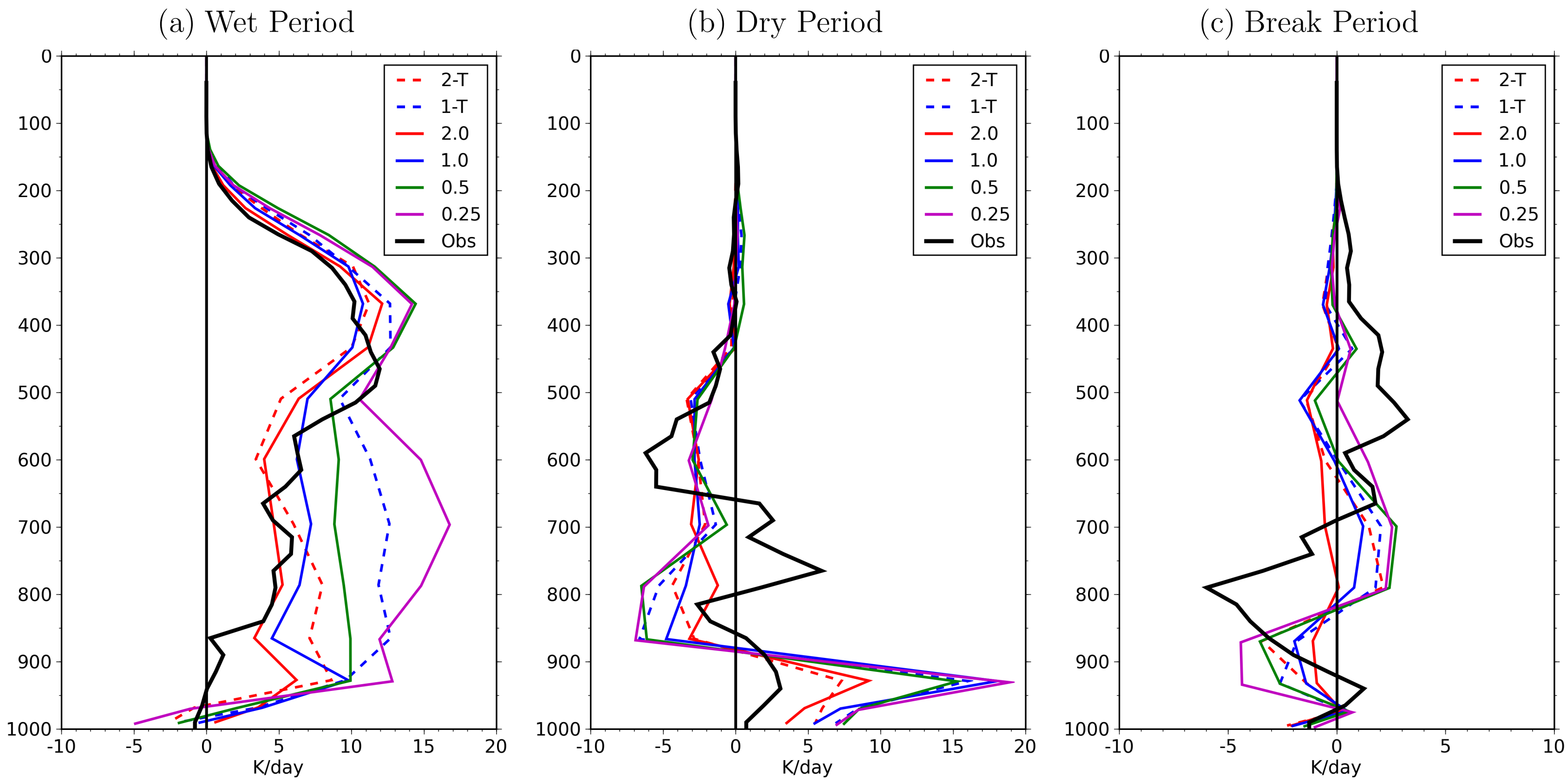

Figure 12. Variational Analysis and modeled apparent drying for the TWP-ICE Wet period. Units are $^{\circ}$K day^{-1}.

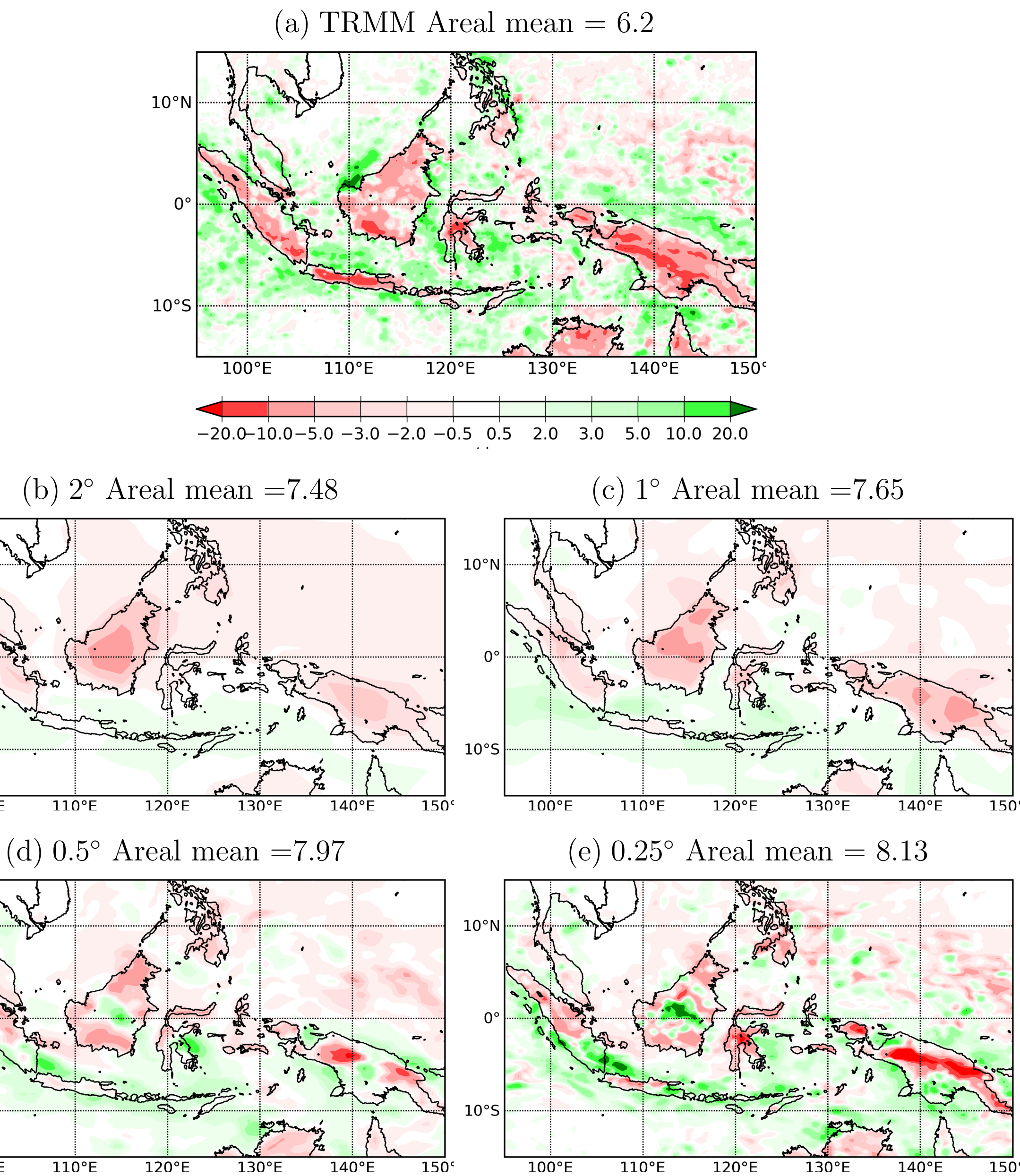

Figure 13. TRMM and modeled precipitation at 00 GMT averaged over January and February 2006 with the daily mean removed. Captions include the mean rainfall over the depicted region. Units are mm day^{-1}.

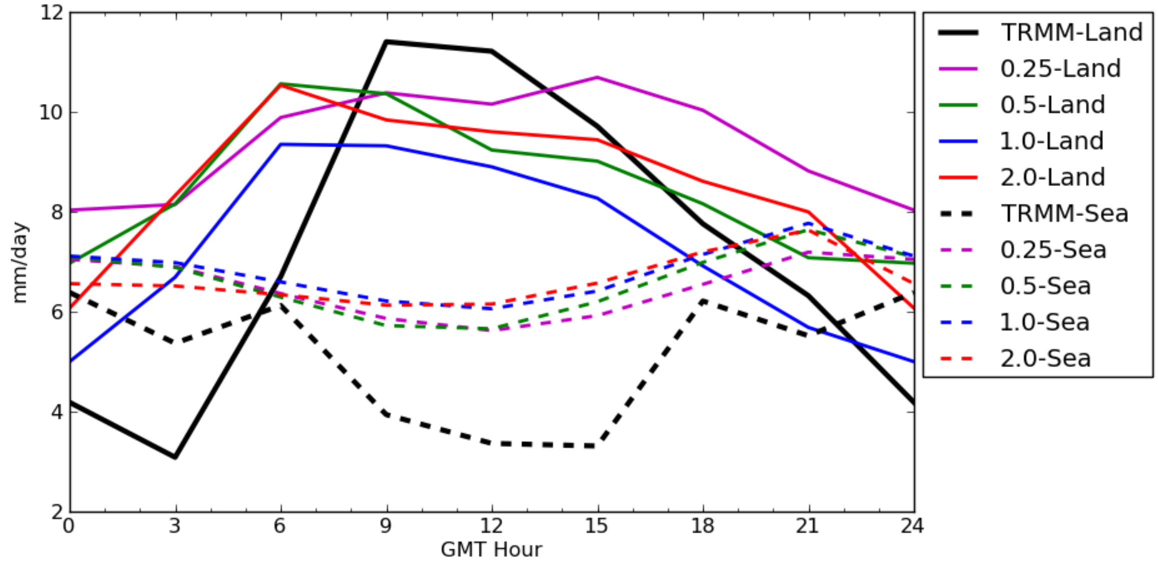

Figure 14. TRMM and model rainfall diurnal cycle averaged for January and February 2006. Data are averaged over land (solid lines) and sea (dashed lines) for the region 15°S to 15°N and 95°E to 130°E . Land (Sea) is determined by a grid box having land (sea) fraction greater the 0.7. 00 GMT corresponds to about 8 AM in this region.

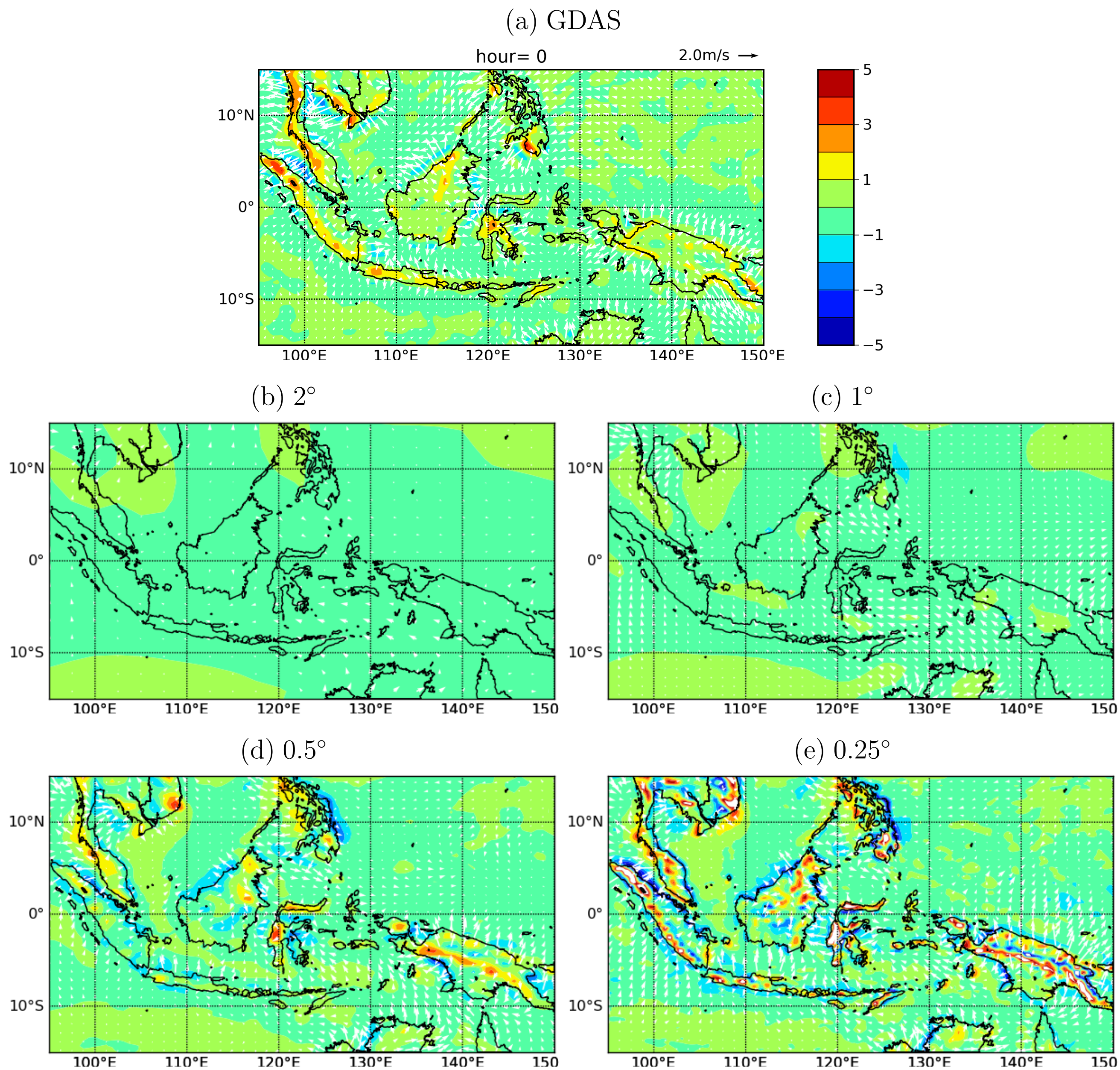

Figure 15. GDAS and modeled surface divergence (colors) and wind (vectors) at 00 GMT averaged over January and February 2006 with the daily mean removed. The scale for the wind is on the upper right of each plot. Divergence units are s^{-1} and wind units are m s^{-1}. For clarity, the vectors are thinned for the higher resolutions.